

A New Version of Flusser Moment Set for Pattern Feature Extraction

Constantin-Iulian VIZITIU, Doru MUNTEANU, Cristian MOLDER

Communications and Electronic Systems Department

Military Technical Academy

George Cosbuc Avenue 81-83, Bucharest

ROMANIA

vic@mta.ro, munteanud@mta.ro, mcc@mta.ro

<http://www.mta.ro>

Abstract: - The choice of a suitable feature extraction method is essential for the success of the classification or recognition process. This paper proposes a design method for a new pattern descriptor set based on the Flusser moment class, which is invariant to elementary geometric transforms and has an increased robustness to the action of some perturbations. Experimental results based on the use of a real video image database confirm the basic properties of this new descriptor set.

Key-Words: - Pattern feature extraction, Flusser moment class, pattern recognition, neural network

1 Introduction

To be useful in a *pattern recognition* process, the objects or patterns resulting from the segmentation of an input image must be represented in a suitable manner [7], [8], [10].

This specific pattern representation assumes some basic *properties* like: concision, redundant information discarding, invariance to elementary geometric (or affine) transforms and conservation of relevant information for pattern recognition applications [11], [15].

Accordingly, this process known as *feature extraction* is in a straight connection with the structure chosen for the input data representation, and is strongly dependent on the implemented applications [10], [12].

In the fundamental literature assigned to the theory of digital image processing, a lot of suitable standard and neural methods for pattern feature extraction are mentioned [2], [3], [6], [9]. Having as a starting point the high level of classification performances offered by the use of *geometric moment* class, an interesting approach in the field of recognition systems is represented by the Flusser moment class [4], [13].

The use of *standard* Flusser moments inside of a recognition system leads to very good classification performances [4], but this approach has some

important disadvantages, such as: average robustness to noisy factors, deficiencies for symmetrical input images etc. However, an improved version of the standard Flusser moments that corrects most of these difficulties must be considered [5].

The aim of this paper is to provide a design procedure for a *new* invariant set belonging to the Flusser moment class, which represents an improved and more robust alternative solution to the reference standard moments. In the first part of the paper, a theoretical demonstration of the design algorithm, as well as basic properties of this new invariant set is presented. In the last part of the paper the experimental results that confirm the theoretical properties of the proposed invariant set are shown. Finally, some important conclusions and future research are also included.

2 Design Procedure for Proposed Invariant Set

The design procedure for the proposed invariant set starts with the basic definition of the $(p+q)^{\text{th}}$ - order *complex moment* for an integral function $f(x, y)$ [1]:

$$c_{pq} = \int_{-\infty}^{\infty} \int_{-\infty}^{\infty} (x+iy)^p (x-iy)^q f(x,y) dx dy \quad (1)$$

$$p, q \in \mathbb{Z}^+$$

According to [4], it can be demonstrated that:

$$c_{pq} = \sum_{k=0}^p \sum_{s=0}^q \binom{p}{k} \binom{q}{s} (-1)^{q-s} \cdot i^{p+q-k-s} \cdot m_{k+s, p+q-k-s}, \quad p, q \in \mathbb{Z}^+ \quad (2)$$

where m_{pq} is given by equation:

$$m_{pq} = \int_{-\infty}^{\infty} \int_{-\infty}^{\infty} x^p y^q f(x,y) dx dy, \quad p, q \in \mathbb{Z}^+ \quad (3)$$

and represents the $(p+q)^{th}$ -order standard geometric moment [11].

In [4], the following significant theorem has been demonstrated (*Flusser theorem*):

“If the following conditions are met: $n \geq 1$

and $\sum_{j=1}^n k_j (p_j - q_j) = 0, \quad k_j, p_j, q_j \in \mathbb{Z}^+,$ then the

product $I = \prod_{j=1}^n c_{p_j q_j}^{k_j}$ is rotation invariant”.

The most important disadvantage of the above descriptor set $\{I_k\}_k$ is given by the fact that this set is not invariant to all elementary geometric transforms.

An immediate and efficient solution to this problem could be the substitution $m_{pq} \rightarrow \eta_{pq}$ in equation (2):

$$c_{pq}^{(1)} = \sum_{k=0}^p \sum_{s=0}^q \binom{p}{k} \binom{q}{s} (-1)^{q-s} \cdot i^{p+q-k-s} \cdot \eta_{k+s, p+q-k-s}, \quad p, q \in \mathbb{Z}^+ \quad (4)$$

where η_{pq} is given by equation:

$$\eta_{pq} = \int_{-\infty}^{\infty} \int_{-\infty}^{\infty} (x-x_c)^p (y-y_c)^q f(x,y) dx dy, \quad (5)$$

$$p, q \in \mathbb{Z}^+$$

and represents the $(p+q)^{th}$ -order centered geometric moment. Also, it is known that (x_c, y_c) are the coordinates of the input pattern centroid [7].

Consequently, considering this substitution as a starting point, the translation and scaling invariance of η_{pq} moments (according to [7]), and applying the theoretical results from Flusser theorem, we can demonstrate that this new descriptor set $\{I_k^{(1)}\}_k$ is invariant to elementary geometric transforms (translation, scaling, and rotation).

For normal conditions, this pattern description generates complex values. Therefore, to obtain real values, we can retain, for example, either its real part, or imaginary part.

To obtain the final form of the proposed invariant set, a new type of $(p+q)^{th}$ order complex moment must be considered, according to the following equation:

$$\lambda_{pq} = \int_{-\infty}^{\infty} \int_{-\infty}^{\infty} (x-x_c+x_s)^p (y-y_c+y_s)^q \cdot f(x,y) dx dy, \quad p, q \in \mathbb{Z}^+ \quad (6)$$

where the *shift factors* x_s and y_s are chosen according to [7], and are given by the equation:

$$x_s = \sqrt{\frac{\eta_{20}}{m_{00}}}, \quad y_s = \sqrt{\frac{\eta_{02}}{m_{00}}} \quad (7)$$

Moreover, the new central moment set can be normalized to ensure its translation and scale invariance using the following equation:

$$\xi_{pq} = \frac{\lambda_{pq}}{m_{00}^{\frac{p+q}{2} + 1}}, \quad p, q \in \mathbb{Z}^+ \quad (8)$$

It has been demonstrated that, using the above shift factors, the most important advantage is the discarding of the standard central moment deficiencies when using symmetrical images as

system inputs, simultaneously with the enhancement of the sensibility to the noise action [11].

A similar replacement as the one from equation (3) leads to an improved structure of the proposed moments:

$$c_{pq}^{(2)} = \sum_{k=0}^p \sum_{s=0}^q \binom{p}{k} \binom{q}{s} (-1)^{q-s} i^{p+q-k-s} \cdot \xi_{k+s, p+q-k-s}, \quad p, q \in \mathbb{Z}^+ \quad (9).$$

Therefore, the *final form* of the proposed invariant set can be rewritten as it follows:

$$\left\{ \begin{array}{l} \zeta_1 = c_{11}^{(2)} \\ \zeta_2 = c_{21}^{(2)} c_{12}^{(2)} \\ \zeta_3 = \operatorname{Re} \left(c_{20}^{(2)} c_{12}^{(2)2} \right) \\ \zeta_4 = \operatorname{Im} \left(c_{20}^{(2)} c_{12}^{(2)2} \right) \\ \zeta_5 = \operatorname{Re} \left(c_{30}^{(2)} c_{12}^{(2)3} \right) \\ \zeta_6 = \operatorname{Im} \left(c_{30}^{(2)} c_{12}^{(2)3} \right) \\ \zeta_7 = c_{22}^{(2)} \\ \zeta_8 = \operatorname{Re} \left(c_{31}^{(2)} c_{12}^{(2)2} \right) \\ \zeta_9 = \operatorname{Im} \left(c_{31}^{(2)} c_{12}^{(2)2} \right) \\ \zeta_{10} = \operatorname{Re} \left(c_{40}^{(2)} c_{12}^{(2)4} \right) \\ \zeta_{11} = \operatorname{Im} \left(c_{40}^{(2)} c_{12}^{(2)4} \right) \end{array} \right. \quad (10).$$

The moment set given by equation (10) has the following *four* important properties:

- elementary geometric transforms (rotation, translation and scaling) invariance;
- elimination of the standard central moment deficiencies in case of symmetrical image use;
- robustness to the action of noisy factors inside of a recognition system, better than the use of standard Flusser moments;
- independent base of pattern invariants (in the sense of the Flusser theorem).

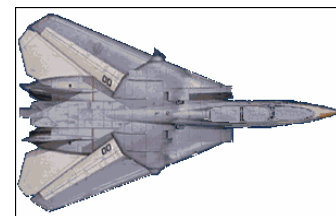
The theoretical properties of the proposed invariant set are confirmed by the experimental results presented in the next section of the paper.

3 Experimental Results

The main *objectives* of these experiments are:

- demonstration of basic properties of the proposed moment set, according to the theoretical background presented in the previous paragraph;
- a comparative study with the standard Flusser moments as reference, to evaluate the performance level of a recognition system that will use these feature extraction methods (in fact, it is important to evaluate the robustness to digital image processing specific noise).

The input video database used in the first part of the paper consists of *two* prototype-images of modern military aircrafts, as it can be seen in Fig.1.



Eurofighter



Mirage 2000

Fig.1: Prototype-images of video database used in the first experimental section (Top view)

Each prototype-image has a resolution of 128x128 pixels, in an uncompressed BMP format.

To test the elementary geometric transforms invariance of the proposed invariant set, each prototype-image was translated, scaled and rotated according to [11]. The results obtained after the moment calculus given by equation (10) are shown in Table 1.

Therefore, the invariance property of the proposed invariant set is obtained (the relative close values from the shady rows in Table 1). One explanation for the small differences that appear between these values is the computing errors caused by the MATLAB internal working algorithm.

To analyze the behavior of the proposed

invariant set to the action of different symmetries existing in the input images, a collection of *standard testing* images has been used [11]. The results after the calculus of the moments given by equation (10) are shown in Table 2.

We can observe that the *deficiencies* of the standard central moments for symmetrical input images (odd rank moments are zero) are eliminated (see, for example, the non-zeros values from shady rows in Table 2).

Table 1

Transform Moment		Reference images	Translation (pixel number)		Scaling (scaling factor)		Rotation (degree)	
			25	50	1.5	2	90°	180°
ζ_1	Eurofighter	-9.88e+003	-9.88e+003	-9.88e+003	-10e+003	-9.82e+003	-9,84e+003	-9,88e+003
	F16	-4.96e+003	-4.96e+003	-4.96e+003	-4.93e+003	-4.90e+003	-4,87e+003	-4,96e+003
ζ_2	Eurofighter	-8.62e+010	-8.62e+010	-8.62e+010	-8.76e+010	-8.52e+010	-8.57e+010	-8.58e+010
	F16	6.96e+005	6.96e+005	6.96e+005	6.92e+005	6.73e+005	6.83e+005	6.95e+005
ζ_3	Eurofighter	8.52e+014	8.52e+014	8.52e+014	8.65e+014	8.37e+014	8.47e+014	8.48e+014
	F16	2.94e+009	2.94e+009	2.94e+009	2.87e+009	2.78e+009	2.91e+009	3.12e+009
ζ_4	Eurofighter	-5.53e+006	-5.53e+006	-5.53e+006	-5.49e+006	-5.55e+006	-5.43e+006	-5.51e+006
	F16	1.48e+007	1,48e+007	1,47e+007	1.43e+007	1.38e+007	1.41e+007	1.50e+007
ζ_5	Eurofighter	7.43e+021	7.43e+021	7.43e+021	7.68e+021	7.27e+021	7.34e+021	7.36e+021
	F16	-1.17e+012	-1.17e+012	-1.17e+012	-1.21e+012	-0.95e+012	-1.23e+012	-1.20e+012
ζ_6	Eurofighter	3.21e+008	3.21e+008	3.22e+008	3.25e+008	3.34e+008	3.1e+008	3.25e+008
	F16	4.23e+009	4.23e+009	4.23e+009	4.27e+009	4.22e+009	4.31e+009	4.27e+009
ζ_7	Eurofighter	2.60e+008	2.61e+008	2.61e+008	2.66e+008	2.56e+008	2.52e+008	2.60e+008
	F16	6.39e+007	6.39e+007	6.39e+007	6.29e+007	6.22e+007	6.51e+007	6.42e+007
ζ_8	Eurofighter	-2.25e+019	-2.25e+019	-2.25e+019	-2.33e+019	-2.21e+019	-2.20e+019	-2.23e+019
	F16	-3.78e+013	-3.78e+013	-3.78e+013	-3.82e+013	-3.63e+013	-3.85e+013	-3.81e+013
ζ_9	Eurofighter	5.34e+011	5.34e+011	5.34e+011	5.39e+011	5.37e+011	5.27e+011	5.38e+011
	F16	-2.15e+008	-2.15e+008	-2.15e+008	2.10e+008	2.12e+008	2.20e+008	-2.17e+008
ζ_{10}	Eurofighter	1.94e+030	1.94e+030	1.94e+030	2.04e+030	1.92e+030	1.87e+030	1.92e+030
	F16	2.24e+019	2.24e+019	2.24e+019	2.32e+019	2.34e+019	2.27e+019	2.31e+019
ζ_{11}	Eurofighter	6.74e+002	6.74e+002	6.75e+002	6.81e+002	6.77e+002	6.83e+002	6.72e+002
	F16	3.21e+004	3.21e+004	3.21e+004	3.27e+004	3.25e+004	3.30e+004	3.23e+004

Experimental results obtained for invariance testing

Table 2

Moment	The type of symmetry							
	Symmetry referred at both axes		Symmetry referred at x axis		Symmetry referred at y axis		Symmetry referred at centroid	
	O	O	D	D	U	U	Z	Z
ζ_1	0.36	0.38	0.31	0.33	0.32	0.35	0.45	0.45
ζ_2	2.10e-006	1.97e-006	1.55e-005	1.62e-005	9.70e-005	10.2e-005	1.82e-005	1.93e-005
ζ_3	3.71e-008	3.82e-008	-1.34e-007	-1.21e-007	1.60e-006	1.47e-006	-3.69e-006	-3.71e-006
ζ_4	1.15e-007	0.98e-007	1.19e-007	1.14e-007	2.79e-004	2.70e-004	-1.91e-006	2.01e-006
ζ_5	3.88e-013	3.78e-013	-1.19e-009	-1.05e-009	-2.87e-008	-2.91e-008	7.62e-010	-7.65e-010
ζ_6	9.50e-013	9.43e-013	2.28e-009	2.24e-009	-7.62e-009	-7.58e-009	-9.48e-010	-9.43e-010
ζ_7	0.14	0.16	0.11	0.138	0.132	0.152	0.27	0.27
ζ_8	1.19e-008	1.23e-008	-1.76e-007	-1.81e-007	2.09e-006	2,19e-006	-1.92e-006	-1.86e-006
ζ_9	3.71e-008	3.67e-008	1.57e-007	1.61e-007	3.55e-007	3.58e-007	-1.38e-006	-1.42e-006
ζ_{10}	1.83e-014	1.81e-014	-1.10e-012	-0.98e-012	-4.91e-010	-4.97e-010	-2.97e-012	-2.95e-012
ζ_{11}	-1.31e-014	-1.27e-014	7.16e-012	7.27e-012	-1.73e-010	1.76e-010	-3.31e-011	-3.28e-011

Experimental results obtained for standard central moment deficiency discarding

Another important aspect is a comparative study between the invariant set given by equation (10) and the standard Flusser invariant set used as a reference to reveal the noise robustness.

The logical diagram used to generate the input video database for neural classifier training and testing is presented in Fig.2.

As we can see from Figure 2b, the video database used in this application was obtained from a (digital) photographical survey of *five* modern military aircraft models (F117, Mirage 2000, Mig 29, F16 and Tornado) scaled at 1:48. The survey was taken using a 5° increment in the azimuthal plane, using a range of $[0^{\circ}, 180^{\circ}]$ justified by the geometric aircraft shape symmetry.

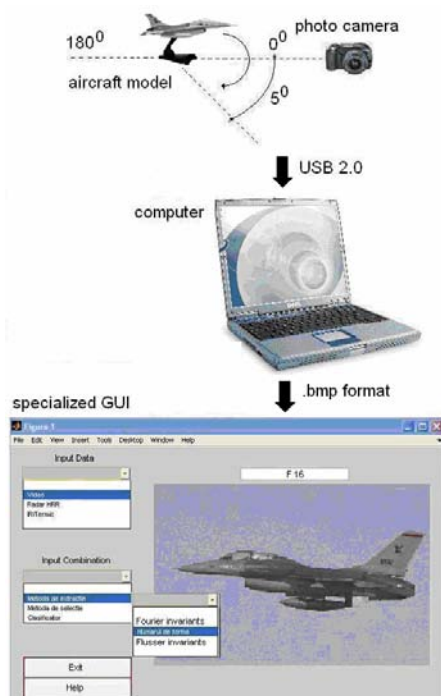


Mirage 2000

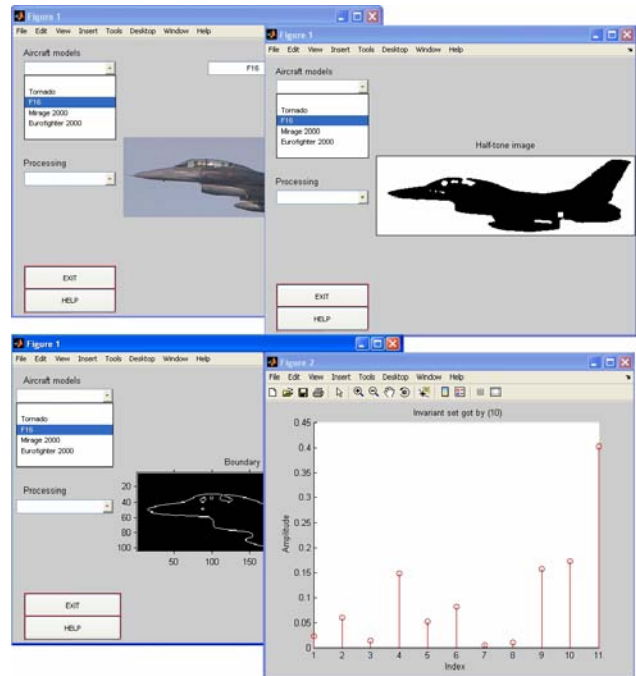


F 16

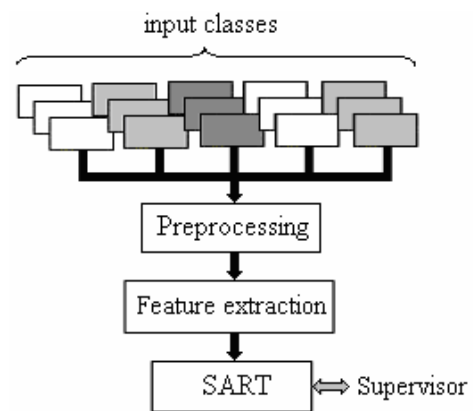
a) Examples of military aircraft models used in video database design



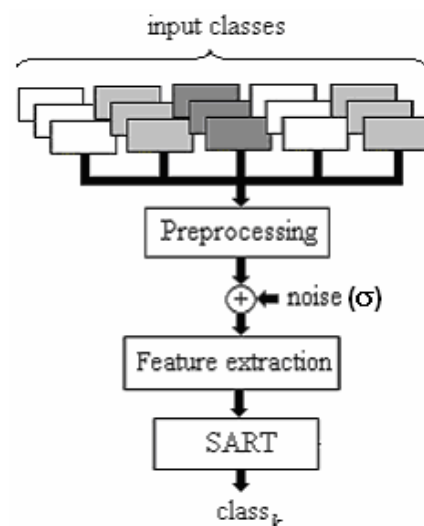
• Basic acquisition and preprocessing diagram



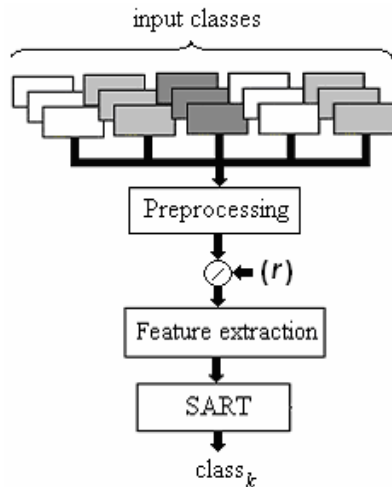
• Examples of calculus procedures from GUI
a) Acquisition and preprocessing GUI
b) Acquisition and preprocessing step



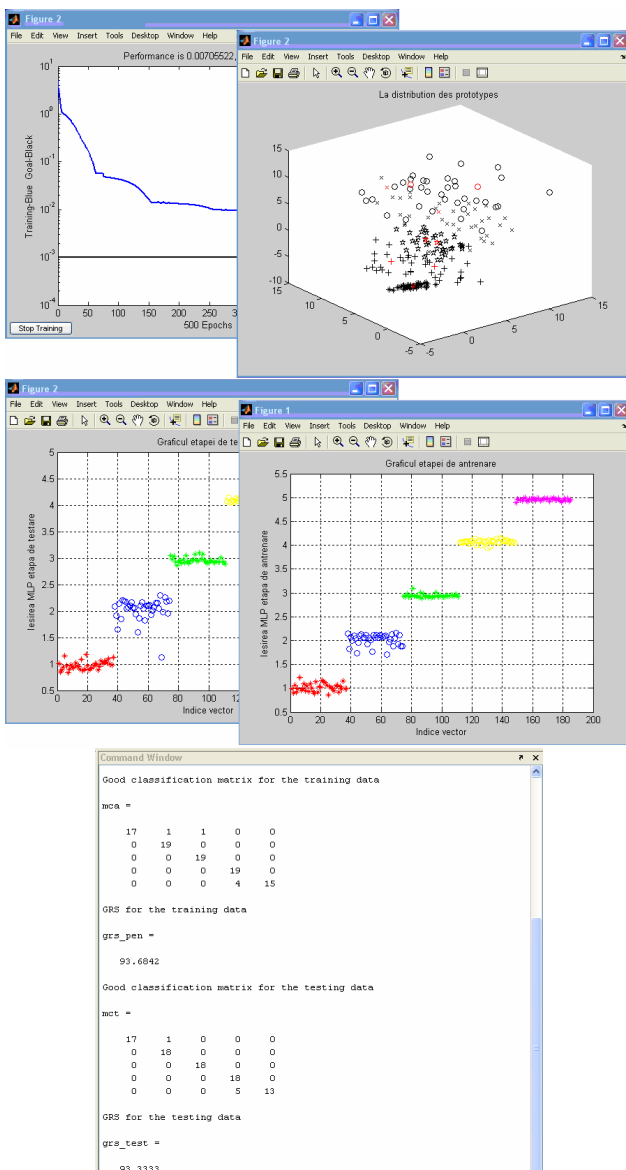
• Classifier training substep



• Noise adding and classifier testing substep



- Variable resolution and classifier testing substep



- Examples of calculus procedures from GUI (Classifier learning GUI)
 - c) Perturbation adding and classification step
- Fig.2: The testing procedure of robustness

Each image from the input video database has a resolution of 520×160 pixels, in an uncompressed BMP format.

A supervised ART artificial neural network (SART) was used for classification purposes [12].

The SART classifier uses the principle of prototype generation similar to ART neural network but, unlike this one, the prototypes are generated in a supervised manner. It has the capability of fast learning using local approximations of the class and its operation does not depend on any chosen parameter.

The idea is to create a new prototype for a class whenever the actual set of prototypes is not capable anymore to classify the training data set satisfactorily. The prototypes are updated using the mean of the samples which are correctly classified by each of them. The updating process is repeated as long as there are classification errors on the training samples and as long as it dynamically changes the location of the prototypes.

Speaking in terms of probability distribution, the prototypes become the centroids of the modes of the multimodal class probability distribution.

The classifier structure is similar to that of an RBF or LVQ neural network. The algorithm described above is then used to train hidden layer, while a MADALINE network implements the output layers (see Fig.3).

An important property of the SART neural algorithm is that it needs no initial system parameter specifications and no prespecified number of codebook vectors.

According to [12], a short version of the standard SART algorithm is indicated in Table 3. Also, the neural classifier structure is shown in Fig.3.

Table 3

<i>Step 1: Initialization</i>	
§	a randomly selection of a vector as prototype for each input class
§	initialization of the vector list associated to each class prototype
<i>Step 2: Learning</i>	
§	while there are changed prototypes and the error rate is higher than a preset value
	For each vector belong to an input class
	→ the vector is compared with the actual prototypes and classified
	If the vector is correct classified
	→ the vector is added to the list assigned to the winner prototype
	If the vector is not correct classified
	→ the vector is declared as new prototype and the initial vector list is updated

Table 3 (cont.)

Step 2: Learning
Update the prototypes assigned to each class
The prototype is recalculated as average between the vectors that are associated with its own list
Check if some prototypes have changed
Eliminate the prototypes for that associated vector list contains only a vector
Exit if the number of maxim iterations or prototypes is reached
§ the neuronal weights of the output layer are calculated using the pseudo-inverse method or Widrow-Hoff algorithm

SART classifier standard algorithm

After the acquisition and preprocessing step (see Fig.2b), a number of 37 video images per class is obtained. Using an interlacing splitting method on input video database, a number of 19 images were used for SART neural classifier training, while for testing 18 images were used.

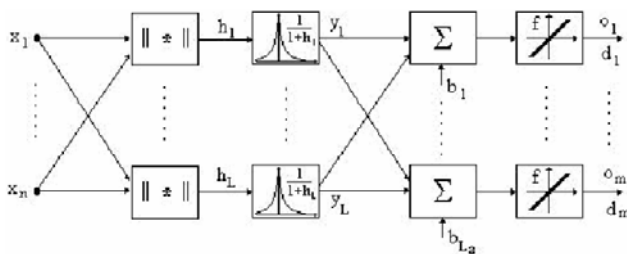


Fig.3: SART neural classifier structure

To quantify the recognition system (or ATR system) performances, each database image was mixed in testing substep with *salt and pepper* noise (it is known that this noise is characteristic for a digital image processing chain), with σ dispersion as a control parameter, modified into $[0, 0.1]$ range with a 10^{-2} increment (see Fig.2c and 4a).

To test the robustness of the proposed invariant set for input images with digital variable resolution (it is known that, for example, for a video homing missile system, the variable digital resolution simulates the variation of the relative distance between the missile video sensor and the current target from its field of view), the real dimensions of each database image were also divided in testing substep with a suitable *ratio*, with r as a control parameter, modified into $\{1, 2, 4, 8, 10\}$ set (see Fig.2c and 4b).

Usually, a serious decrease of classification performances is expected when the input database images are affected by these perturbation factors [8].

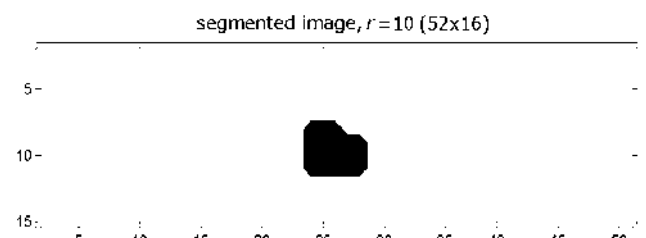
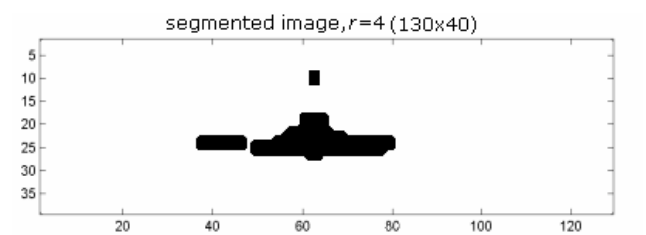
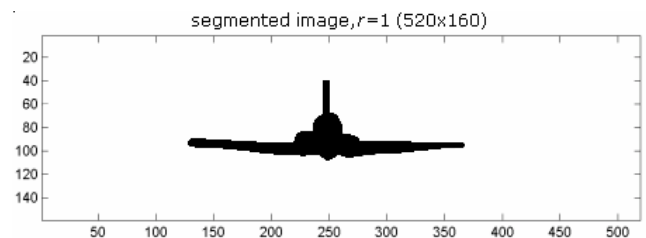
After the SART classifier training and testing steps, it is important to quantify and analyze the perturbation factor influence on the recognition system performances by moment calculus. Therefore, the GRS (*good recognition score*) has been computed, as it is the most important performance indicator. The GRS represents, in %, the



• Unnoisy input database image ($\sigma=0$)



• Input database image after noise adding ($\sigma=0.1$)
a) *Salt and pepper* noise adding substep



b) Influence of *variable resolution* on pattern shape

Fig.3: Influence of tested perturbation factors on input database image quality

the ratio between the number of correct classified input patterns and the total number of patterns used for classification.

In Fig. 4 a graphical representation of the resulted $GRS = f(\sigma)$ dependence is shown.

As we can see, the moments given by equation (10) have a higher value of noise robustness than the standard Flusser moments.

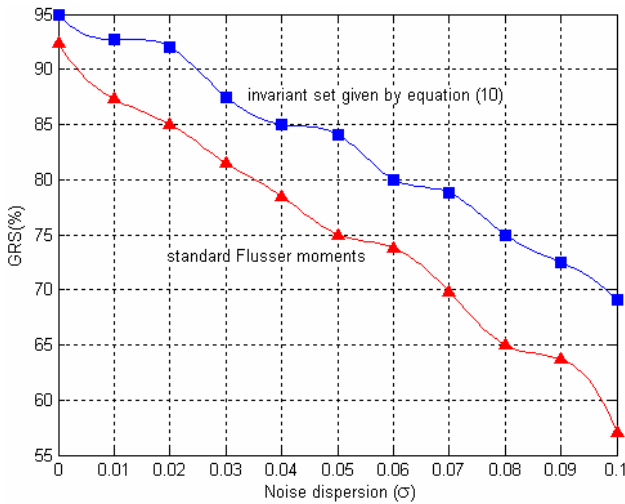


Fig.4: $GRS = f(\sigma)$ dependence

In Fig.5, using a proper interpolating *spline* algorithm, a graphical representation of the resulted $GRS = f(r)$ dependence is shown.

As we can see, only for a ratio r less than 5.5, the proposed invariant set has a higher value of variable resolution robustness than the reference Flusser moments. However, this aspect is not very important because, in practice, we can consider an *effective* or *real* recognition system (ATR system) if its GRS is more than 50 % (see Fig.5).

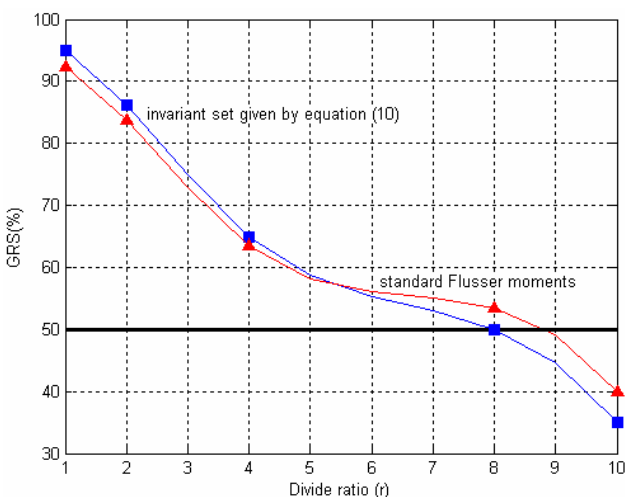
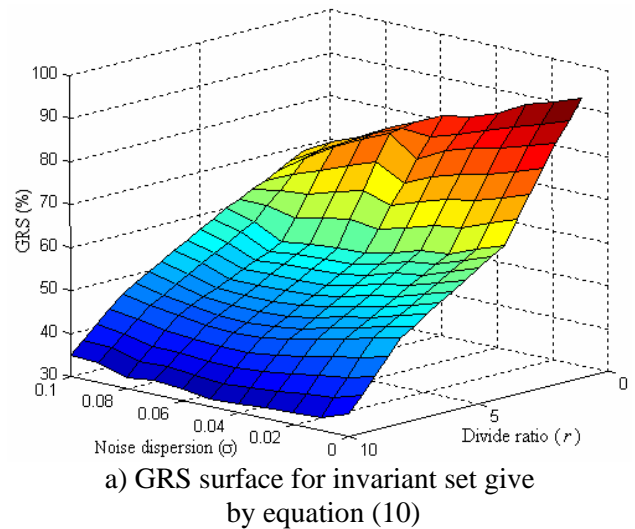
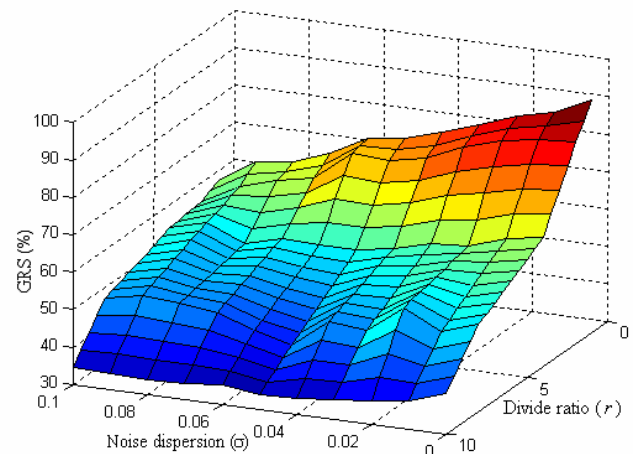


Fig.5: $GRS = f(r)$ dependence

Another interesting experimental result of the above applications is the possibility to draw the GRS surfaces for the invariant set give by equation (10) and respectively, standard Flusser moments. In the context of the present work, a GRS surface represents a graphical representation of $GRS = f(\sigma, r)$ dependence (see Fig.6).



a) GRS surface for invariant set give by equation (10)



b) GRS surface for standard Flusser moments
Fig.6: $GRS = f(\sigma, r)$ dependence

As we can see from Fig.6, the GRS surface shape is relatively similar, but in case of standard Flusser moments use, this is more stirring and its slope is more slanted than invariant give by equation (10) use. Generally speaking, this observation based on GRS surface shape analysis is an additional demonstration of proposed invariant set superiority to perturbations comparing to the reference set.

To prove that the proposed invariant set forms an *independent base* (accordingly to Flusser theorem), a proper feature selection method was applied on the video image database obtained after the acquisition and preprocessing step. The selection method is an

improved version of Sammon projection algorithm on a $R^{11} \rightarrow R^n$ form.

The *new* form used for *normalized* error or *stress* definition assigned to standard Sammon algorithm can be rewritten as it follows (according to [9], using this modified version of standard Sammon algorithm, a serious increasing of feature selection step performances is expected):

$$E^{new} = \frac{1}{\sum_{i=1}^{N-1} \sum_{j=i+1}^N d_{ij}^{p+2}} \sum_{i=1}^{N-1} \sum_{j=i+1}^N d_{ij}^p (d_{ij} - \delta_{ij})^2 \quad (11),$$

$p \in Z$

where $d_{ij}, i, j = \overline{1, N}$ describes the distance between either points of n dimensional input space (in our case, this value is 11), $d_{ij}, i, j = \overline{1, N}$ describes the distance between either points of m dimensional output space, N is the point number from input map and, p is a parameter used for Sammon normalized error minimization.

According to [14], using the parameter p , the intraclass variance can be minimized and respectively, the interclass variance can be maximized. Also, in order to increase the computing speed, this nonlinear projection algorithm was initialized with the final projection solution given by PCA algorithm [7], [13].

A short version of the generalized Sammon projection algorithm is presented in Table 4.

Table 4

Step 1: Initialization
§ using PCA solution, the vectors from output space are initialized
Step 2: Projection calculus
§ the distances between either points of n dimensional input space are calculated
§ using previous calculus, the distances between either points of m dimensional output space are calculated
§ in order to minimize the Sammon stress, the optimal value for parameter p is determined
§ according to equation (11), the Sammon stress is calculated
§ if the Sammon stress is more than a preset value → stop else

Table 4 (cont.)

Step 2: Projection calculus
→ the output vector map is recalculated
→ go to substep used for Sammon stress minimization
end

Generalized Sammon projection algorithm

This late experiment searches for informational redundancy inside the moment set given by equation (10). If by preserving (or increasing) the classification performances (see first row in Table 5), the projection space dimension can be decreased (less than 11) then the proposed invariant set does not form an independent base for pattern recognition.

The classification results using the same classification diagram as the one from Fig.2 are presented in Table 5.

Table 5

Feature selection	Classification performances
is not applied ($m = 11$)	GRS: 95% SART training parameters: eradm= 10^{-2} ; nepmax=10; nprmax=10 Training/testing time: 3.5 s
is applied ($m = 10$)	GRS: 78% SART training parameters: eradm= 10^{-2} ; nepmax=10; nprmax=10 Training/testing time: 3.1 s
is applied ($m = 3$)	GRS: 52% SART training parameters: eradm= 10^{-2} ; nepmax=10; nprmax=10 Training/testing time: 1.8 s

Classification results after Sammon projection

As we can see from Table 5, trying to reduce the feature space dimension can lead to much lower GRS values comparing to the case with no feature selection. Fig.7 shows the 3D input data projection. The structure of the output data does not allow a very good classification. Consequently, it results that the invariants given by equation (10) form an independent base for pattern recognition [4].

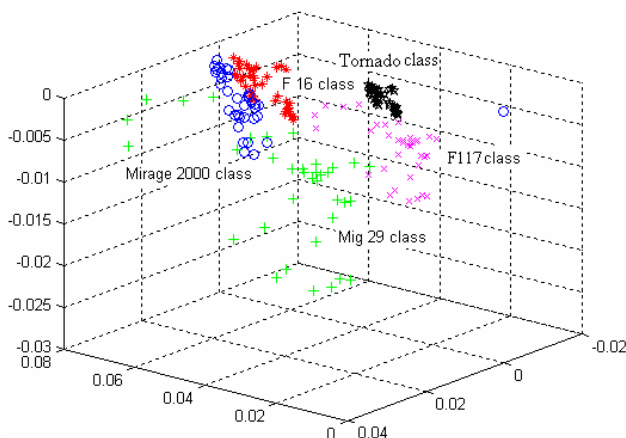


Fig.7: Database 3D Sammon projection
(Accordingly with the last row from table 5)

More details regarding experimental aspects treated in this section can be found in [14].

4 Conclusion and Future Work

The theoretical and experimental results presented in this paper leads to the following *remarks* concerning the basic properties of the proposed moment set:

- the moment set given by equation (10) is elementary geometric transforms invariant, it eliminates the central moments deficiencies for symmetrical input images, it is more robust to perturbations comparing to standard Flusser moments, and it forms an independent base for pattern recognition;

- when this set is used as a feature extraction method in a classification system (ATR system), and in case of noise absence, the GRS are greatly improved, generally 4% more than the standard Flusser moments. For noise adding case, the GRS are also very good, generally 7% more than the reference moment set (see Fig.4). Finally, for input images with variable resolution use and respectively, for divide ratio less than 5.5, the GRS are good, generally 2% more than the standard Flusser moment (see Fig.5);

- the computing resources required are relatively lower than those for the standard Flusser moment calculus.

As a final conclusion, the design of the proposed moment set as a feature extraction method inside of recognition system (ATR system) is *feasible*. Also, the invariants given by equation (10) represent an important and robust *alternative* as well as performance, not only for Flusser moment class, but for all geometric moments.

In a future improvement, the comparative study of the proposed invariant set and the standard Flusser moments will be extended to a larger class of pattern

description methods, [11], [15]. Accordingly, it will be interesting to make a comprehensive comparison as well as performance, between invariants given by equation (10) and other well-known descriptor classes (e.g., Zernike moment class, Hu moment class, improved Flusser moments etc.).

Also, it will be interesting to analyze and quantify the behavior (in terms of GRS and robustness) of the proposed invariants when the perturbation factors are changed. For example, it is important to know what is the robustness level of this invariant set for other types of noises which are specific to a digital processing chain (particularly, the noises by multiplicative type).

Another interesting point for a future development refers to integration of the invariants given by equation (10) into a new classification scheme. For example, some possible classification schemes can be: {neural version of the generalized Sammon algorithm and a genetic optimized feedforward neural network} or {ICA technique and a neuro-fuzzy network}.

In the same scientific research direction, is will be useful to make a more serious experimental analysis concerning the GRS surface shape properties in connection with classification and/or robustness performances of recognition system. Accordingly, as a result of GRS surface analysis, it will be possible to identify the optimal classification schemes for different types of real ATR systems, [14].

References:

- [1] A. Abo-Zaid, O. Hinton, and E. Horne, "About moment normalization and complex moment descriptors", *Proceedings of ICPR Conference*, pp. 399-407, 1988
- [2] J. Adams, E. Curtis, "Feature Extraction Methods for Form Recognition Applications", *WSEAS Transactions on Information Science and Applications*, vol.3, issue 3, pp.666-671, ISSN 1790-0832, 2006
- [3] C. Aviles, A. Garcia, "Image Searching based on Principal Components Analysis and Invariant Moments", *WSEAS Transactions on Information Science and Applications*, vol.3, issue 10, pp.2066-2078, ISSN 1790-0832, 2006
- [4] J. Flusser, "On the Independence of Rotation Moments Invariants", *Pattern Recognition Journal*, no.33, pp.1405-1410, 2000
- [5] J. Flusser, T. Suk, "Rotation Moment Invariants for Recognition of Symmetric Objects", *IEEE Transaction on Image*

- Processing*, vol.15, pp. 3784-3790, ISSN: 1057-7149, 2006
- [6] A. Foulonneau, P.Charbonnier, "Affine-Invariant Geometric Shape Priors for Region-Based Active Contours", *IEEE Transactions on Pattern Analysis and Machine Intelligence*, vol.28, no.8, pp.1352-1357, 2006
- [7] R. Gonzales, R.E. Woods, *Digital Image Processing*, Second Edition, Prentice Hall, 2002
- [8] A. Jain, *Fundamentals of Digital Image Processing*, Prentice-Hall International Inc., Englewood Cliffs, 1990
- [9] R.I. Maheb, "Application of Neural Networks Analysis in Image Feature Extraction", *WSEAS Transactions on Information Science and Applications*, vol.2, issue 7, pp.945-950, ISSN 1790-0832, 2005
- [10] M.S. Nixon, A.S. Aguado, *Feature Extraction in Computer Vision and Image Processing*, ELSEVIER, 1st Edition, USA, 2002
- [11] M. Rodrigues, *Invariants for Pattern Recognition and Classification*, World Scientific Publishing Co., Danvers, 2000
- [12] I.C. Vizitiu, *Neural Networks used in Pattern Recognition*, MTA Publishing House, Bucharest, 2005
- [13] I.C. Vizitiu, "A New Approach to Increase the Video Pattern Recognition Performances", *International Symposium on Defense Technology*, ZMNDU, pp. 416-443, Budapest, Hungary, 2006
- [14] I.C. Vizitiu and collective, *Smart Multisensor System for Automatic Air Target Tracking and Recognition*, Scientific Research Report of CNCSIS grant, AT type, no. 88 GR, pp. 145-153, 2006-2007
- [15] D.Xu, H.Li, "Geometric moment invariants", *Pattern Recognition Journal*, No.41, pp.240-249, 2008